Toxicology and Applied Pharmacology 295 (2016) 56–67

Contents lists available at ScienceDirect

Toxicology and Applied Pharmacology

journal homepage: www.elsevier.com/locate/ytaap

BFD-22 a new potential inhibitor of BRAF inhibits the metastasis of B16F10 melanoma cells and simultaneously increased the tumor immunogenicity

Adilson Kleber Ferreira [a,c,*], Kerly Fernanda Mesquita Pasqualoto [b], Frank A.E. Kruyt [c], Fanny Palace-Berl [d], Ricardo Alexandre Azevedo [a], Kely Medeiros Turra [e], Cecilia Pessoa Rodrigues [a], Ana Carolina Franco Ferreira [a], Maria Alejandra Clavijo Salomón [a], Paulo Luiz de Sá Junior [f], Camyla Fernandes Farias [g], Carlos Rogerio Figueiredo [g], Leoberto Costa Tavares [d], José Alexandre Marzagão Barbuto [a,h], Salomão Dória Jorge [a,*]

[a] Laboratory of Tumor Immunology, University of São Paulo, São Paulo, SP, Brazil
[b] Biochemistry and Biophysics Laboratory, Butantan Institute, São Paulo, SP, Brazil
[c] Department of Medical Oncology, University of Groningen, University Medical Center Groningen, Hanzeplein 1, Groningen, The Netherlands
[d] Laboratory of Drug Design and Development, University of São Paulo, São Paulo, SP, Brazil
[e] Laboratory of Cytopathology, Department of Clinical Chemistry and Toxicology, Faculty of Pharmaceutical Sciences, University of São Paulo, São Paulo, SP, Brazil
[f] Laboratory of Genetics, Butantan Institute, São Paulo, SP, Brazil
[g] Experimental Oncology Section, The Federal University of São Paulo, São Paulo, SP, Brazil
[h] Cell and Molecular Therapy Center NUCEL-NETCEM, University of São Paulo, SP, Brazil

ARTICLE INFO

Article history:
Received 4 August 2015
Revised 19 January 2016
Accepted 9 February 2016
Available online 10 February 2016

Keywords:
Melanoma
Benzofuroxan derivatives
Cell death
Anti-metastatic
BFD-22

ABSTRACT

Benzofuroxan is an interesting ring system, which has shown a wide spectrum of biological responses against tumor cell lines. We investigated, herein, the antitumor effects of benzofuroxan derivatives (BFDs) *in vitro* and in a melanoma mouse model. Cytotoxic effects of twenty-two BFDs were determined by MTT assay. Effects of BFD-22 in apoptosis and cell proliferation were evaluated using Annexin V-FITC/PI and CFSE staining. In addition, the effects in the cell cycle were assessed. Flow cytometry, western blot, and fluorescence microscopy analysis were employed to investigate the apoptosis-related proteins and the BRAF signaling. Cell motility was also exploited through cell invasion and migration assays. Molecular docking approach was performed in order to verify the BFD-22 binding mode into the ATP catalytic site of BRAF kinase. Moreover, the BFD-22 antitumor effects were evaluated in a melanoma murine model using B16F10. BFD-22 was identified as a potential hit against melanoma cells. BFD-22 induced apoptosis and inhibited cell proliferation of B16F10 cells. BFD-22 has suppressed, indeed, the migratory and invasive behavior of B16F10 cells. Cyclin D1 and CDK4 expression were reduced leading to cell cycle arrest at G0/G1 phase. Of note, phosphorylation of BRAF at Ser338 was strongly down-regulated by BFD-22 in B16F10 cells. The accommodation/orientation into the binding site of BRAF was similar of BAY43-9006 (co-crystallized inhibitor of BRAF, sorafenib). Importantly, BFD-22 presented *in vivo* antimetastatic effects and showed better therapeutic efficacy than sorafenib and taxol. BFD-22 can be considered as a new lead compound and, then, can be helpful for the designing of novel drug candidates to treat melanoma.

1. Introduction

Malignant melanoma is an aggressive and highly metastatic form of skin cancer, resistant to the majority of therapeutic antitumor agents currently used (Monge-Fuentes et al., 2014; Tomei et al., 2014). Mortality rates due to melanoma have been increasing during the last decades, now affecting about 150,000 new patients per year in the world (Lens and Dawes, 2004; Li et al., 2014). Despite the fact that melanoma presents resistance to the conventional chemotherapeutics, a significant increase in the survival time has been obtained through the surgical removal of the primary lesion. The surgical procedure may either cure patients in the early stages of melanoma or increase survival rates in advanced stages of disease (Wevers and Hoekstra, 2013). Currently, the options for the treatment of melanoma have remained limited, in spite of the advances in immunotherapy and targeted therapy, to the

Abbreviations: BAY43-9006, sorafenib; BFD, *substituted*-[*N*′-(benzofuroxan-5-yl) methylene]benzohydrazides; BFD-22, 3,4-dichloro-[*N*′-(benzofuroxan-5-yl)methylene] benzohydrazides.

* Corresponding authors at: Av. Prof Lineu Prestes, 1730, ICB IV, Cidade Universitaria - Butanta, Sao Paulo, SP 05508-000, Brazil.
E-mail addresses: ferreira-kleber@usp.br (A.K. Ferreira), sdjorge@usp.br (S.D. Jorge).

http://dx.doi.org/10.1016/j.taap.2016.02.008
0041-008X/

use of BRAF inhibitors (Weise and Flaherty, 2014). The individual characterization of molecular/genetic lesions in melanoma will certainly provide targets in order to develop more useful therapy (Smith et al., 2014). Indeed, the relative lack of success of the existing treatments against metastatic melanomas turns the development of new and more effective drugs extremely urgent (Johnson et al., 2014).

The designing and development of new drugs demand years of research and efforts of multidisciplinary teams, making it an expensive endeavor (Adams and Brantner, 2010). On the other hand, the screening of already available small molecules could also be considered as a starting point and financially accessible alternative, which could lead to the discovery and development of promising novel antitumor agents, even when the mechanism of action is initially unknown (Mader, 2005). Benzofuroxan (benzofurazan oxide; benzo [1,2-*c*]1,2.5-oxadiazole *N*-oxide) is a well-known and quite interesting ring system, which has shown a wide spectrum of relevant biological activities, such as antiprotozoal, antifungal, platelet antiaggregatory, and NO-releasing activity. Then, this kind of compounds can provide promising new drug candidates (Cerecetto and Porcal, 2005; Cerecetto and González, 2007). The presence of the ═N(→O)O— moiety in benzofuroxan derivatives confers electron-accepting properties to the molecule similarly to those containing aromatic *N*-oxides (Šarlauskas et al., 2009), such as tirapazamine, which are used as bioreducible antitumor and/or cytotoxic agents (Brown, 1993). Since the first report in the 1960s, when Ghosh and Whitehouse had shown the use of 4-nitrobenzofuroxan as an inhibitor of nucleic acid and protein biosynthesis in animal cells (Ghosh and Whitehouse, 1968), a variety of benzofuroxan derivatives were synthesized and evaluated for its antitumor activity, and these compounds have recently been reviewed (Jovene et al., 2013).

Our group has previously reported the anti-proliferative activity of a set of substituted-[*N*′-(benzofuroxan-5-yl)methylene]benzohydrazides (BFDs) against epimastigote forms of *Trypanosoma cruzi* (Jorge et al., 2012; Jorge et al., 2013), showing no genotoxic activity against human fibroblasts cells (FN1) and human bronchial epithelial cells (HBEC). Recently, we have also demonstrated the putative therapeutic potential of BFD-22 combined with sorafenib against lung cancer (Teixeira et al., 2014).

In this study, the antitumor activity of BFDs was explored in several tumor cell lines as well as in B16F10 mouse melanoma model. BFDs were assayed in order to verify their cytotoxic activity in several tumor cell lines, and the most promising compounds, BFD-22, has been selected for further testing in melanoma cells. BFD-22 has induced mitochondrial depolarization and caspase-3 cleavage, which led to apoptosis of B16F10 cells *in vitro*. Additionally, BFD-22 has inhibited cell migration and invasion of melanoma cells and was also able to potentially inhibit melanoma lung metastasis in the B16F10 model. We have also demonstrated that BFD-22 is not toxic against Bone Marrow Dendritic cells (BMDC), besides it has been suggested that BFD-22 might induce dendritic cells (DCs) maturation. Thus, although speculative, considering the immune system as a powerful weapon against cancer, we may suggest that the BFD-22 treatment not only induces their anti-tumoral activity upon cancer cells but also *via* their effects upon the DCs, which seems to bend the later toward an immunogenic bias. BFD-22 was able to inhibit B-RAF/C-RAF heterodimer formation and it, in turn, reduced the translocation of RAF to the plasma membrane. To further evaluate this finding, a molecular docking approach was carried out into the ATP catalytic site of BRAF kinase. Interestingly, the accommodation/orientation into the BRAF binding site was similar for both inhibitors, BFD-22, and BAY43-9006 (co-crystallized inhibitor, sorafenib). Overall, BFD-22 has potentially antitumor effects and can be considered as a promising new lead for the development of anti-melanoma drug candidates.

2. Materials and Methods

2.1. Chemicals

The substituted-[*N*′-(benzofuroxan-5-yl)methylene]benzohydrazides (BFDs) were previously synthesized. The general structure and simplified code names of the compounds are shown in Table 1, and the synthetic procedures and chemical structure data can be found elsewhere (Jorge et al., 2009; Jorge et al., 2011; Jorge et al., 2012; Jorge et al., 2013).

Table 1
In vitro cytotoxicity data of benzofuroxan derivatives (BFDs).

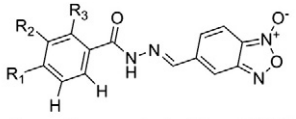

benzofuroxan derivatives (BFD)[a]

1 R_1 = H
2 R_1 = CH_3
3 R_1 = NH_2
4 R_1 = OH
5 R_1 = F
6 R_1 = CN
7 R_1 = C_2H_5
8 R_1 = OCH_3
9 R_1 = Cl
10 R_1 = $COCH_3$
11 R_1 = *n*-C_3H_7
12 R_1 = *iso*-C_3H_7
13 R_1 = $N(CH_3)_2$
14 R_1 = *n*-C_4H_9
15 R_1 = *tert*-C_4H_9
16 R_1 = OC_3H_7
17 R_1 = CF_3
18 R_1 = OC_4H_9
19 R_1 = Br
20 R_1 = I
1 - 20 R_2 = R_3 = H
21 R_1 = Cl, R_2 = H, R_3 = Cl
22 R_1 = Cl, R_2 = Cl, R_3 = H

Code	B16F10	A2058	GRANTA-519	MCF-7	NIH-3T3	Melan-A
1	25.3	29.7	31.73	28.8	75.8	38.8
5	16.7	51.1	28.23	15.7	53.3	27.4
10	25.4	42.8	23.66	24.0	49.9	47.8
17	9.7	26.4	NA	8.6	31.7	13.4
19	12.1	17.5	22.95	12.0	22.7	12.5
20	8.3	17.4	24.55	NA	10.1	13.5
21	19.6	59.4	8.06	28.3	62.6	29.3
22	8.0	18.3	17.68	8.2	25.3	8.4

[a]Chemical structures of benzofuroxan derivatives.
*The results are presented in triplicate [SD (standard deviation) <10% for all cases] and represents the IC50 values in μM. NA represent an IC50 value >200 μM.

2.2. Cell culture

B16F10 (mouse skin melanoma), A2058 (human skin, melanoma, metastatic), MCF-7 (human breast cancer), Granta-519 (mantle cell lymphoma), and NIH 3T3 (mouse embryonic fibroblast) cell lines were obtained from the American Type Culture Collection (Mannasa, VA, USA). Melan-A (melanocytes) cell line was kindly provided by Dr. Alisson Leonardo Matsuo from the Federal University of São Paulo (UNIFESP). All cell lines were cultured in the RPMI-1640 medium, supplemented with 10% fetal bovine serum, penicillin (100 units/mL), streptomycin (100 mg/mL), at 37 °C, in a humidified atmosphere with 5% CO_2 (de Azevedo et al., 2014).

2.3. MTT colorimetric assay

Cells were plated in 96-well flat bottom tissue culture plates at 1×10^4 cells/100 μl/well concentration. The cells were allowed to grow for 24 h and treated with concentrations of benzofuroxan (from 10 μM to 100 μM). After 24 h treatment, cell viability was determined by MTT (3-[4.5 dimethylthiazol-2-yl]-2,5diphenyltetrazolium bromide). Briefly, MTT reagent (Sigma-Aldrich, St. Louis, USA) (20 μL) was added to each well in order to reach a final concentration of 5 mg/mL, incubated for 4 h at 37 °C, and then centrifuged at 2000 rpm for 10 min (Ferreira et al., 2014). After that, the medium was discarded, and dimethyl sulfoxide (100 μL) was added to each well. Each experiment was performed using six replicates for each drug concentration and performed in triplicate.

2.4. Cell cycle analysis

B16F10 cells were synchronized by deprivation of serum for 24 h and, then, induced to *re*-enter the cell cycle by subsequent addition of serum. After that, cells were treated for 12 and 24 h with the compound BFD-22 (8 μM). Then, the cells were collected and fixed, permeabilized with cold 70% ethanol and stored at −20 °C (Canon et al., 2015). Subsequently, cells were washed, *re*-suspended in PBS, and incubated at 37 °C for 45 min with 10 mg/mL RNase and 1 mg/mL Propidium Iodide (SIGMA, St. Louis, MO). The percentage of cells in the different cell cycle phases was determined using a FACScalibur flow cytometry system (Becton Dickinson, San Jose, CA), and analyzed using Modfit LT software (Verity Software House, Topsham, ME).

2.5. Cell proliferation assay

B16F10 cells were incubated with carboxyfluorescein succinimidyl ester (CFSE; Molecular Probes, Inc., Eugene, OR) at 0.5 μM for 10 min at room temperature (Ferreira et al., 2013). Then, cells were washed twice with complete medium, and culture plates were seeded with 10^4 cells/mL in 24-well. After cell adhesion, the compound BFD-22 (8 μM) was added for 48 h, and cell proliferation was analyzed by flow cytometry using a FACScalibur flow cytometry system. The cell proliferation analysis was carried out using Flowjo version 8.7. The data were reported as "division index" from four independent experiments.

2.6. Apoptosis assay

For the evaluation of apoptosis, the cells were plated in 6-well culture plates, grown overnight and treated with BFD-22 (8 μM). The adherent and floating cells were collected and washed in PBS. The cells were, then, centrifuged and cell pellets were re-suspended in binding buffer (100 μL), and stained with Annexin V-FITC/PI (Geeraerts et al., 2007), apoptosis detection kit (BD Bioscience). After 30 min incubation, the binding buffer (400 μL) was added, and cells were analyzed by flow cytometry using FACScalibur and CellQuest software, in order to determine the percentage of apoptotic cells. A minimum of events (10,000) was acquired for each sample in three independent experiments.

2.7. Caspase-3 activity fluorometric assay

B16F10 cells 1×10^5 were treated with BFD-22 (8 μM) for 12 h. After that, cells were lysed in 100 μL of buffer 1×, collected and stored at −7 °C until analysis. Briefly, it was added buffer 1× (3 mL) to each well, and incubated at 37 °C for 5 min. Caspase activity was measured in three independent experiments, in triplicate, using caspase-3 fluorometric assay kit from Biovision (Milpitas, CA) (Ahmed et al., 2013). The number of cells was determined by using a CytoFluor II PerSeptive Biosystems (Farmington, MA) fluorometric plate reader, with excitation at 360 nm and emission at 460 nm.

2.8. ROS detection assay

B16F10 cells (10^6 cells/well) were seeded in 6-well plates and incubated for 12 h prior to the treatment with BFD-22 (8 μM or 16 μM) for 12 h. Then, cells were harvested and washed once with PBS prior to adding the substrate dihydrorhodamine 123 (DHR 123, Invitrogen, Eugene, USA). After that, cells were incubated for 15 min at 37 °C, washed once with PBS, and kept at 4 °C during ROS measurements, using the FACScalibur (Richardson et al., 1998). A total of 10,000 cells/sampled was acquired in three independent experiments, each one performed in triplicate, and the mean of fluorescence intensity was recorded.

2.9. Wound-healing assay

B16F10 (5×10^5 cells/well) were grown to confluence in a 12-well plate, placed in medium containing 1% serum for 24 h at 37 °C. Then the cell layer was scratched with a sterile plastic tip and washed twice with serum free medium (Shen et al., 2014). After that, serum was increased in 5% in order to facilitate cell migration, and cells were immediately treated with BFD-22 (8 μM), for 48 h. Cell migration was recorded using a Nikon TE2000E microscope system (Nikon Instrument). The area of wound healing was calculated as the percent of wound area repaired and, then, it was compared to the initial wound area using Image J software (version 14.1) National Institutes of Health (Bethesda, Maryland, USA) from tree independent experiments.

2.10. Matrigel invasion assay

Matrigel-coated transwell inserts (Becton Dickinson) were used to study cell invasion (Qi et al., 2014). Briefly, the transwell inserts with 8-μm pores were coated with Matrigel (20 μg/well) and 1×10^5 cells in 500 μL were added to the upper chambers in the presence or absence of BFD-22 (8 μM). Then, RPMI medium (700 μL) was added into the lower wells, as chemoattractant. After 24 h treatment, cells that had invaded the bottom of the Matrigel-coated membrane were fixed with 70% ethanol, stained with Giemsa, counted in five random fields under a light microscope and plotted as the percentage of invading cells. Three independent experiments were carried out, each one performed in triplicate.

2.11. Confocal laser scanning microscopy

B16F10 cells were seeded onto sterile glass coverslips in 24-well plates. After 24 h of treatment with BFD-22 (8 μM), the cells were fixed with 3.7% paraformaldehyde and permeabilized in 0.05% Triton-X100 diluted in PBS, containing 10% bovine fetal serum (Freitas et al., 2013). Then, the cells were incubated with Phalloidin-green in the dark, at 37 °C, for 45 min, and gently rinsed twice in PBS. Image acquisition was performed with a confocal laser-scanning microscope (Carl Zeiss LSM 700; Leica, Mannheim, Germany). Post-

acquisition image processing, background correction, adjustment of brightness and contrast, and export to tiff format were done using Image J software (version 14.1) National Institutes of Health (Bethesda, Maryland, USA).

2.12. Generation and culture of Bone Marrow dendritic cells (BMDC)

BALB/c mice male, 6-week-old, were euthanized and their legs separated from the body at hip joint, all muscle tissue were removed from the femur and tibia. After that, bones were washed by puncture the bone end with a needle, and flushing out the bone marrow. Cell suspensions were washed with AIM-V medium (Gibco) and centrifuged for 10 min at 1200 RPM. Then, cells were seeded in Petri dishes and incubated at 37 °C overnight. The non-adherent cells were harvested and centrifuged at 1200 RPM for 10 min. At that time, the cells were counted and seeded at a concentration of 2×10^6 in 6 well plates supplemented with GM-CSF and IL-4 (50 ng/mL), and incubated at 37 °C. After 5 days, typical BMDC attachment was noticed at the plate bottom, and cells were treated with BFD-22 (8 μM) for 24 h. Then, the effects of BFD-22 on BMDC were evaluated. For this purpose, the cells were harvested at Day 7 after receiving maturation stimuli at Day 5 with LPS (500 ng/mL; *Escherichia coli* 0111:B4; Sigma-Aldrich, St. Louis, MO, USA) and BFD-22 (8 μM).

2.13. Immunophenotypic characterization

BMDC cell preparations (2.5×10^5 cells/PBS-BSA 1%) were stained with live/dead dye (V450, Life Technology) and labeled with antibodies against CD11c-PE and I-A^b-FITC (BD, pharmagem). Samples were acquired using a FACSCanto II cytometer (Becton Dickinson, San Jose, CA, USA), and analyzed using FlowJo software ver. 8.7.2 (Three Star) (Clavijo-Salomon et al., 2014; Pinho et al., 2014). At least 20,000-gated events were acquired and analyzed for the frequency of positive cells and median fluorescence intensity (MFI) for each marker. Three independent experiments were carried out, each one performed in triplicate.

2.14. Allogeneic T-cell proliferation

CD3 T cells were isolated from BALB/c spleens obtained from euthanized mice. Spleens were dissociated into single cell suspensions, filtered using 70 μm filters (Corning, NY), followed by a RBC lysis using an osmotic approach. The resulting cells were centrifuged and seeded in a 6-flat-bottom plate with RPMI-10% for 12 h. Non-adherent cells were removed from the culture, most of them being T lymphocytes (Hermann et al., 2014; Lam et al., 2014). After isolation, the T lymphocytes were incubated with 0.5 μM CFSE for 10 min at room temperature. The cells were co-cultured in a 1:10 ratio with allogeneic BMDCs, immature and mature, treated or not with BDF-22 or sorafenib, for five days. The T lymphocytes proliferation control was placed without any stimulation, or using 2.5% of phytohemagglutinin (PHA). After 5 days, CFSE dilution was measured by flow cytometry using a FACSCanto II flow cytometry system (Becton Dickinson, San Jose, CA). The cell proliferation analysis was carried out using FlowJo Software (Tree Star, Inc.).

2.15. Western blot analysis

B16F10 cells were washed with cold PBS and disrupted in Lysis Buffer supplemented with 1 mM PMSF and complete protease inhibitor cocktail tablets (Cell Signaling, Beverly, MA, USA). Lysates were clarified by centrifugation, and protein concentrations were determined by the Bradford method. Equal amounts of protein were combined with sample buffer (50 Mm Tris/HCL, pH 6.8, 2% SDS, 10% glycerol, 5% 2-β-mercaptoethanol), and boiled for 5 min. For analysis, 20 μg of cleared lysates were separated in 8.0% sodium dodecyl sulfate (SDS)-polyacrylamide gels, blotted to PVDF membranes (Millipore, Bedford, UK), blocked for 1 h in 5% milk powder, and incubated with primary antibodies (Joseph et al., 2014). After washing, the primary antibodies (anti-BCL-2, HSP60, cyclin D1, CDK4, phospho ERK1/2, phospho-*c*-Raf (Ser259) and phospho-b-Raf (Ser338)) were revealed using the appropriate horseradish peroxidase (HRP)-conjugated secondary antibody (Cell Signaling), and detected with Lumi-Light Plus Western blotting kit (Roche, Almere, The Netherlands). Equal protein loading was checked using β-actin staining.

2.16. Metastasis assays in vivo

The animal model experiments were carried out in accordance with the guidelines for animal experimentation determined by the Federal University of São Paulo (UNIFESP) and conducted in accordance with the Institutional Animal Ethics Committee (IAEC). B16F10 cells (1×10^6 cells/mouse) were injected into 6-week-old male C57BL/6 mice through the tail vein in order to produce a syngeneic lung melanoma metastases model (Xie et al., 2013; de Azevedo et al., 2014). The animals were randomized and divided into groups ($n = 5$). On the fourth day after tumor cells inoculation, treatment was started with the intraperitoneal administration of BFD-22 (70 mg/kg/day), sorafenib (10 mg/kg/day) or taxol (70 mg/kg/day) (Sigma-Aldrich, St. Louis, USA), and continued for 15 days. After treatment, the mice were euthanized and the lungs were dissected and nodules/metastatic lesions were counted.

2.17. Molecular docking

A molecular docking approach was performed in order to predict a binding mode for the compound BFD-22 in the ATP catalytic site of BRAF kinase. The BRAF co-crystallized structure bound to the 4-{4-[({[4-chloro-3-(trifluoromethyl)phenyl]amino}carbonyl)amino]phenoxy}-*N*-methylpyridine-2-carboxamide inhibitor (BAY43-9006, sorafenib), entry code 1UWH at 2.95 Å resolution (Wan et al., 2004), was retrieved from Brookhaven Protein Data Bank (PDB) (Berman et al., 2000), and used as geometric reference for constructing the biomacromolecule model. This complex was selected due to the topological similarity between the co-crystallized ligand and compound BFD-22. The structures of biomacromolecule and ligand were prepared in the Autodocktools4 software (Morris et al., 2009). Regarding the BRAF molecular model, hydrogen atoms were added and Gasteiger charges were assigned to each atom of the amino acid residues comprising the backbone. Herein, water molecules were not explicitly considered. The three-dimensional affinity and electrostatic grid boxes were generated using AutoGrid version 4 (Morris et al., 2009). The number of grid points was set as $60 \times 60 \times 60$ for the x, y, z axes, respectively, with a grid spacing of 0.38 Å centered on the original ligand in the crystal structure complex (Wan et al., 2004). Lamarckian genetic algorithm (Morris et al., 1998) implemented in AutoDock 4 (Morris et al., 2009) was employed as the search method. The maximum number of energy evaluations was set to 250,000, and six runs were performed. For each independent run, a maximum number of 27,000 GA (genetic algorithm) operations were generated on a hundred individuals single population. Default parameters for operator weights, crossover, mutation, and elitism were considered (0.80, 0.02, and 1.0, respectively). The re-docking approach of the inhibitor (BAY43-9006) co-crystallized with BRAF (PDB ID 1UWH) (Wan et al., 2004) was also performed in order to verify whether the set docking parameters were appropriated and able to recover the known structure of the complex as well as the related interactions.

2.18. Statistical analysis

All values were expressed as mean ± SD. Each value is the mean of at least three independent experiments in each group. One-way analysis of variance (ANOVA) with Tukey Post-Hoc test was carried out in

order to determine significant differences from untreated controls. The asterisk (*) indicates the values that are significantly different from control (**$p < 0.05$ and ***$p < 0.001$).

3. Results

3.1. BFD induces cytotoxicity against a panel of cancer cell lines

The cytotoxicity profile of different BFDs was firstly carried out in a panel of tumor cells and normal NIH-3T3 fibroblasts. The tumor cells were exposed to BFDs at different concentrations for 24 h and, after MTT assays, the IC_{50} values were calculated (Table 1). The compound named BFD-22 has showed the highest toxicity, at low concentrations, on tumor cells. Interestingly, its toxicity on normal NIH-3 T3 and melanocytes was around 1.5–3-fold lower. BDF-22 has presented the most pronounced effect against murine melanoma B16F10 (IC_{50} value = 8.0 μM) and human breast cancer MCF-7 (IC_{50} value = 8.2 μM).

3.2. BFD-22 inhibits proliferation and induces arrest at G0/G1 phase in B16F10 cells

To better understand the anti-proliferative mechanisms, the cell cycle distributions were exploited (Alexandre et al., 2014). Prior to treatment, the cells were synchronized for 24 h by serum starvation. After that, the cells were stimulated to grow by addition of 10% serum and, then, treated with BFD-22 (8 μM). Notably, after 24 h of treatment, B16F10 cells were significantly arrested at G0/G1 phase (***$p < 0.001$), and the percentage of cells in the G2/M phase was drastically reduced (9.7% ± 1.3 *versus* 34.1% ± 2.3, untreated cells; Fig. 1A and B). In order to identify how BFD-22 has induced the accumulation of B16F10 cells at G0/G1 phase, the expression of cyclin D1 and its catalytic partner, CDK4 (Naselli et al., 2014), were checked (Fig. 1C). Interestingly, BFD-22 has inhibited the expression of these proteins providing a mechanism by which BDF-22 induced G0/G1 cell cycle arrest. These findings suggested that BFD-22 has anti-proliferative activity in B16F10 cells by inducing cell cycle arrest.

An aspect that might be involved in the cytotoxic effect of BFD-22 could be the inhibition of cell proliferation. Then, the effect of BFD-22 on melanoma cell proliferation was evaluated by flow cytometry, using the fluorescent probe CFSE (Fig. 2A). After 48 h treatment, BFD-22 (8 μM) has significantly (***$p < 0.001$) affected B16F10 cells proliferation in comparison to untreated cells (Fig. 2B). However, when 2-fold higher concentration was used, BFD-22 did not affect B16F10 cell proliferation.

3.3. BFD-22 inhibits cell migration and invasion

Cancer progression generally depends on the motility and invasive activities acquired by transformed cells (Martin et al., 2014; Garg, 2015). Then, to investigate whether BFD-22 would affect two central characteristics of tumor metastases, migration and invasion experiments were performed (Jandova et al., 2014). According to Fig. 2C, the wound-healing assay showed that the treatment with BFD-22 (8 μM), for 24 h and 48 h, has decreased wound closure by 19% (±3.1) and 18,3% (±1.9), respectively, in comparison to untreated cells. Corroborating with these findings, BFD-22 (8 μM) has decreased about 40% of the invasiveness in a Matrigel assay, showing reduced numbers of invading melanoma cells into the bottom of the coated membrane (Fig. 2D). Of note, syndecan-1, and perlecan, which regulate the cell-to-extracellular matrix interactions (van Dijk et al., 2013), were reduced on the membrane surface of B16F10 cells (Fig. 2E). Taken together, our results have shown that BFD-22 presents anti-proliferative effects

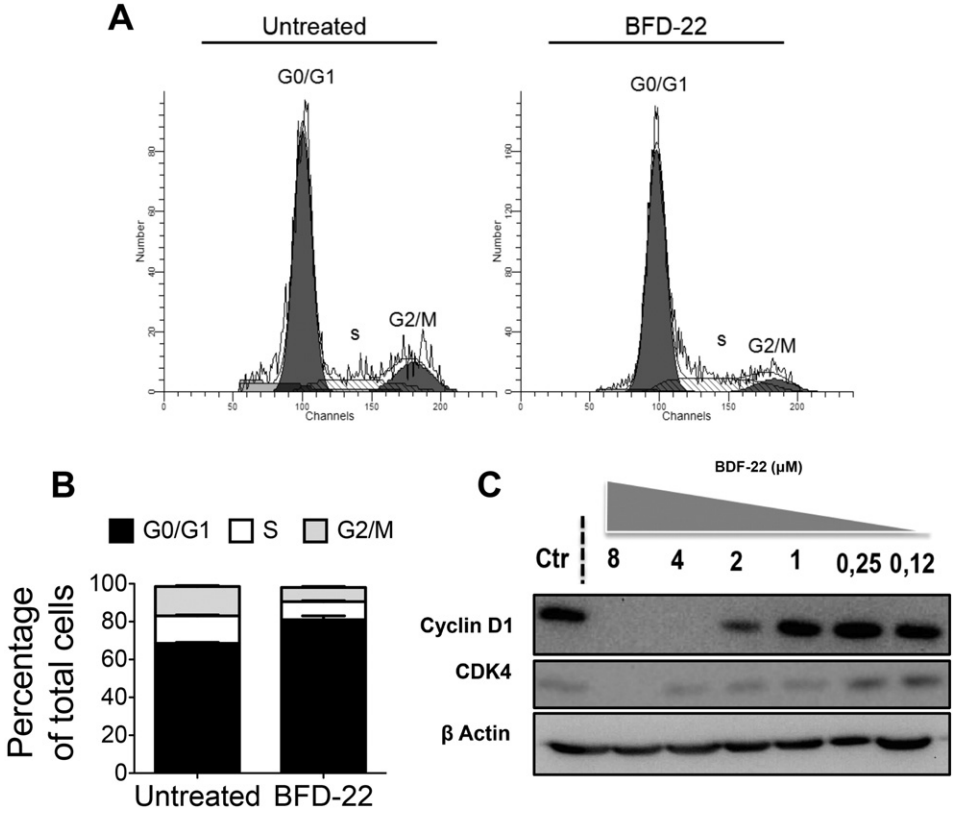

Fig. 1. Inhibition of cell cycle progression of B16F10 cells arrests at G0/G1 induced by BFD-22. (A) Control and BFD-22-treated cells (8 or 16 μM) were stained with propidium iodide and then analyzed by flow cytometry to estimate the number of cells in each phase of the cell cycle. (B) Bar graph indicating the cell cycle distributions of B16F10 cells after treatment with BFD-22. (C) B16F10 cells were treated for 24 h at different concentrations ranging from 0.12 to 8 μM BFD-22. The cyclin D1 and Cdk 4 levels were analyzed by Western blotting with the indicated antibodies. β-Actin was used as loading control. The data are the means ± SD *$P < 0.05$ and **$P < 0.001$ from at least three independent experiments.

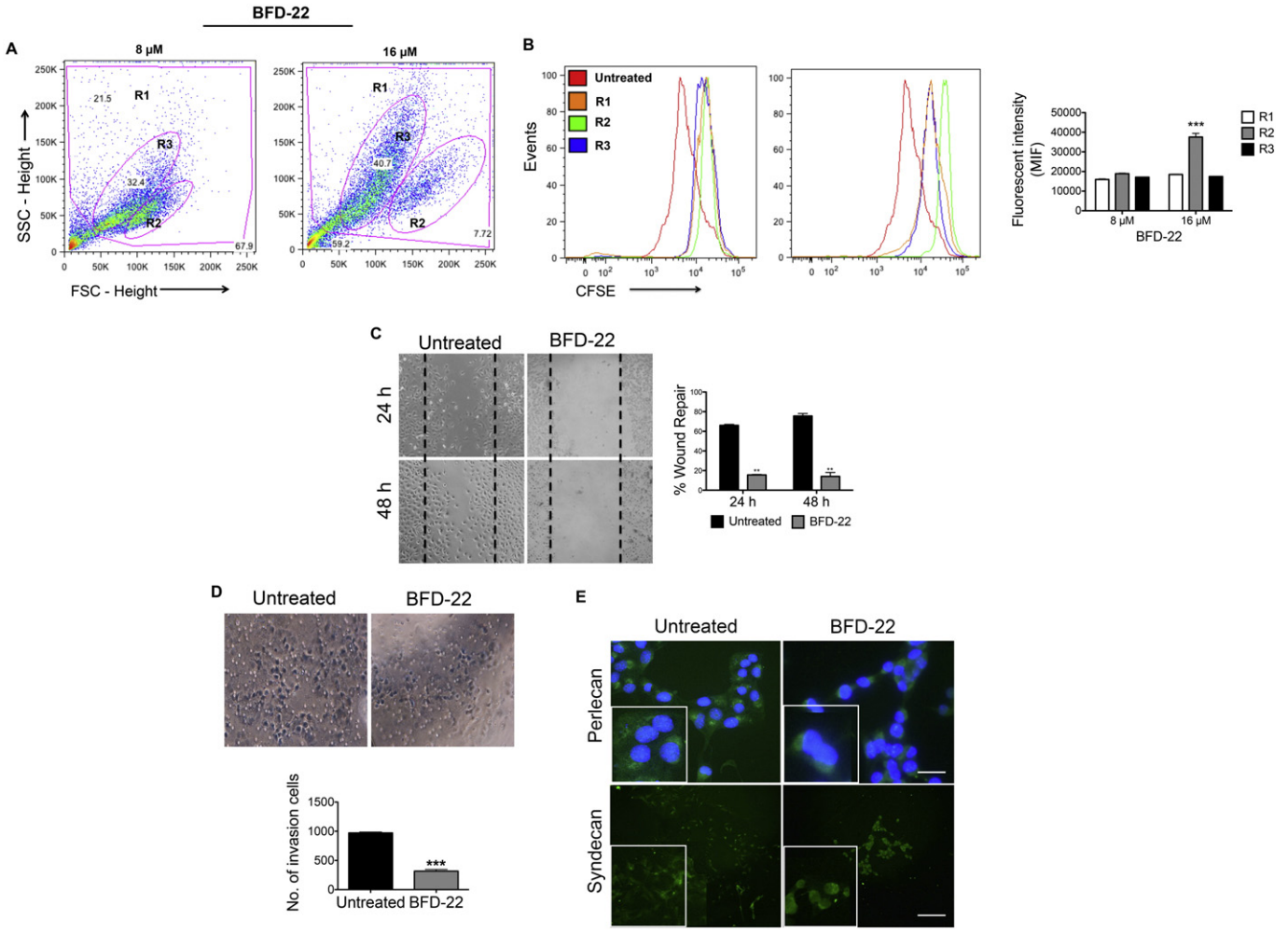

Fig. 2. BFD-22 exhibits *in vitro* an anti-metastatic potential by the inhibition of invasion and migration of B16F10 cells. (A) Control and BFD-22-treated cells (8 or 16 μM) were gated to estimate the cellular morphological features. Assessment of cell proliferation was performed using the CFSE-Proliferation assay. Proliferation capacity was stained with CFSE-labeled and analyzed by flow cytometry. (B) BFD-22-treated B16F10 cells with 16 μM showed lower CFSE staining intensity due to a number of divisions during the 24 h compared to control (untreated). Bar graph indicating the quantification of CFSE intensity of B16F10 cells after treatment with BFD-22. (C) B16F10 cells were treated with BFD-22 8 μM for 48 h and then were wounded, followed by visualization by phase contrast microscopy at indicated times. Images were used to determinate the percentage of wound repair, which was calculated as the percent of wound area compared to the initial scratch. Data are presented as means ± SEM from three independent assays. **, $p < 0.01$ by *t*-test. (D) BFD-22 inhibited invasion in B16F10 melanoma cells. The cells were seeded in the 24-well plate with cell culture inserts, the cells were treated with concentrations of 8 μM for 24 h to test invasion. Bar graph indicating the quantification of the number of invasion cells. **, Indicates $p < 0.01$ *versus* untreated group. Data were shown as means ± SD from three independent experiments. (E) Immunofluorescence microscopy of B16F10 cells treated with BFD-22 8 μM or untreated and incubated for 24 h. The images showed deposition of syndecan and perlecan (green) with nuclei stained with DAPI (blue). Images were taken using a 20× objective.

and, simultaneously, inhibits B16F10 cells migration and invasion, which can affect the metastatic potential of melanoma cells.

3.4. BFD-22 induces apoptosis associated with caspase-3 cleavage and downregulation of HSP60 and Bcl-2

Since our initial screens have identified the compound BFD-22 as a promising anticancer lead to be explored, its mechanism of action against melanoma cells was further investigated. Microscopic analysis of B16F10 cells treated with BFD-22 showed morphological changes typical of apoptosis (Galluzzi et al., 2015), such as cell rounding, membrane blebbing, and vacuolization (data not shown). To investigate this, B16F10 cells were treated with BFD-22 (8.0 μM) for 12 h and then, stained for AnnexinV/PI; the induction of apoptosis was observed in 27.3% (±2.5); $^{**}p < 0.01$ of treated cells (Fig. 3A and B). To further confirm that BFD-22 induces apoptosis in melanoma cells, the DNA integrity of those cells treated with 8 μM or 16 μM, for 12 and 20 h, was exploited (Xu et al., 2015). As shown in Fig. 3C, BFD-22 has increased DNA degradation compared to intact untreated cells. In addition, it was verified whether BFD-22 treatment would be associated with caspase activation in order to induce apoptosis in B16F10 melanoma cells. A fluorimetric assay showed that BFD-22 induced an increase of 55.4% (±2.3) in caspase-3 activation (Thyrell et al., 2002), through cleavage at a specific sequence (*Ac*-YVAD-AMC), in comparison to untreated cells (Fig. 3D). Besides that, it was evaluated whether BDF-22-induced DNA degradation would be correlated to ROS production. In this regard, the releasing of superoxide radicals in B16F10 cells after treatment with BFD-22, 4 μM, and 8 μM, for 12 h, was determined by DHE staining and flow cytometry analysis. Concomitantly with the induction of apoptosis and DNA fragmentation, a significant increase in ROS production determined by MFI was observed in cells treated with BFD-22 (8 μM) ($^{***}p < 0.001$) when compared to the untreated cells (Fig. 3E and F). Augmented ROS levels can be associated with mitochondrial disruption, which can subsequently result in activation of the caspase cascade (Zhou et al., 2014; Boussabbeh et al., 2015). Then, it was evaluated whether BFD-22 could affect mitochondrial permeability transition (MPT), however, prior to the increase in ROS levels, BFD-22 did not affect MPT (Fig. 3G). Thus, BFD-22 does not induce

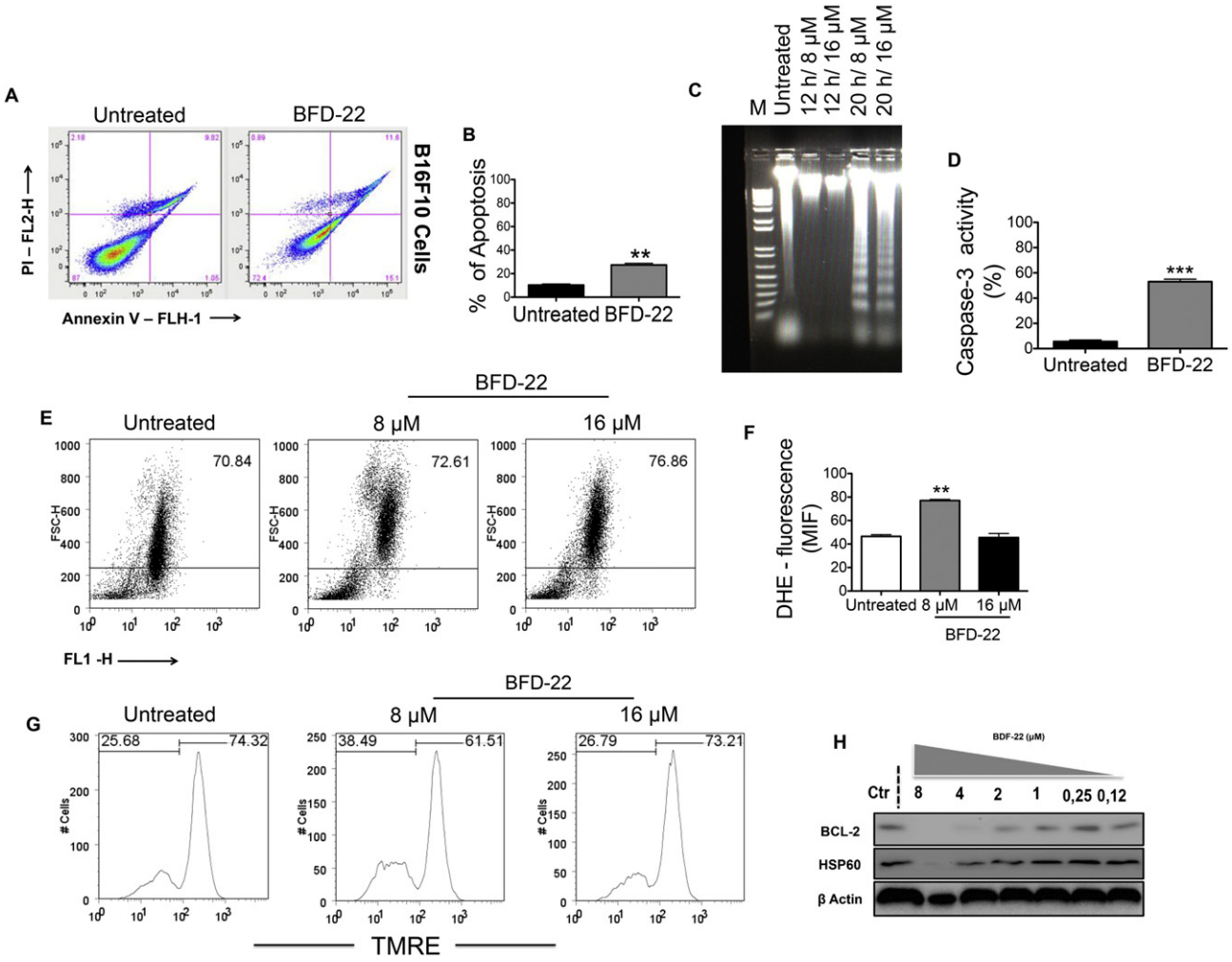

Fig. 3. BFD-22 induces apoptosis in B16F10 cells through oxidative stress and mitochondrial pathway. (A) Apoptosis was evaluated through Annexin V and PI double staining based FACS analysis using the Annexin-V assay kit. (B) Percentage of apoptotic cells were determined by the externalization of phosphatidylserine. (C) DNA fragmentation pattern was evaluated on agarose/EtBr gel. DNA isolated from B16F10 cells treated with BFD-22 or untreated were loaded onto 1% (w/v) agarose gels. Lane 1: Marker (1 kb DNA ladder); Lane 2: DNA isolated from of B16F10 cells untreated; Lane 3: DNA isolated from B16F10 cells treated with 8 µM BDF-22 for 12 h; Lane 4: DNA isolated from B16F10 cells treated with 8 µM BFD-22 for 20 h, Lane 5: DNA isolated from B16F10 cells treated with 16 µM BFD-22 for 12 h. (6) DNA isolated from B16F10 cells treated with 16 µM BFD-22 for 20 h. (D) Caspase-3 activity was measured on B16F10 cells after treatment with 8 and 16 µM BFD-22, by cleavage of the fluorescence peptide substrate DEVD-MCA. (E) A representative FACS profile of cells stained with dihydroethidium (DHE) is shown. (F) B16F10 cells were treated with BFD-22 (8 or 16 µM) and fluorescence intensity of dihydroethidium (DHE) dyes as detected FACS. (G) Loss of mitochondrial membrane potential on B16F10 cells. Control and BFD-22-treated cells (8 or 16 µM) were stained with tetramethylrhodamine ethyl ester (TMRE) and fluorescence was measured by flow cytometry. (H) The BCL-2 and HSP60 levels were analyzed by Western blotting with the indicated antibodies. β-Actin was used as loading control. Data are pooled from two to three independent experiments and values are mean ± SEM ($^{*}p < 0.01$, $^{**}p < 0.001$, $^{***}p < 0.0001$) was determined by ANOVA ($n = 3$).

mitochondrial depolarization to trigger apoptosis of B16F10 cells (Lu et al., 2014). To elucidate the dominant mechanism of apoptosis induced by BFD-22, B16F10 cells were treated with decreasing concentrations, starting from IC_{50} values. First, the expression of Bcl-2, a central anti-apoptotic regulator of mitochondrial cell death (Sarangi et al., 2013; Ye et al., 2014), was investigated. Notably, the Bcl-2 expression in B16F10 cells treated with BFD-22 (8 µM) was abolished after 24 h of treatment. Recently, a molecular chaperone Hsp60 has been reported to play a role in apoptosis and promotion of cancer cell survival (Hjerpe et al., 2013). Interestingly, in B16F10 cells treated with BFD-22 (8 µM), an important decrease of Hsp60 expression was detected. This finding indicates a possible disruption of either Hsp60-p53 or Hsp60-BCL-2, complex (Ghosh et al., 2008).(Fig. 3H).

3.5. BRAF is downregulated in B16F10 cells and docking studies have revealed that BFD-22 binds in its active site

It has been reported that RAF kinase inhibitors have substantial therapeutic effects in patients with BRAF-mutant melanoma (Goetz et al., 2014; Wada et al., 2014). Herein, it was investigated if BFD-22 would affect RAF kinases and ERK1/2 phosphorylation by western blotting. The findings have shown that BFD-22 induces the phosphorylation of Thr202 and Tyr204 ERK in melanoma cells. Furthermore, it was verified if the high activation levels of ERK1/2 might result in an increase in RAF activity (Long et al., 2014). Interestingly, BFD-22 has induced C-RAF stabilization through phosphorylation of its key residue, Ser259, at 1, 2 and 3 h after treatment. Considering the findings, an increment of BRAF activation through the ERK1/2 pathway suggests that, in turn, melanoma cell proliferation and survival would increase (Boussemart et al., 2014). Interestingly, B16F10 cells showed strong down-regulation of BRAF phosphorylated at Ser338 after treatment with BFD-22 among 1 and 2 h (Fig. 4A). The results indicated that BFD-22 can interrupt cell growth signaling and suppress melanoma proliferation through BRAF down-regulation (Caputo et al., 2014). To further support this finding, molecular docking studies were performed in order to evaluate the binding mode of compound BFD-22 into the BRAF active site. Docking procedures have showed that compound BFD-22 fits well in the active site, and in a similar orientation to that found for inhibitor BAY43-9006

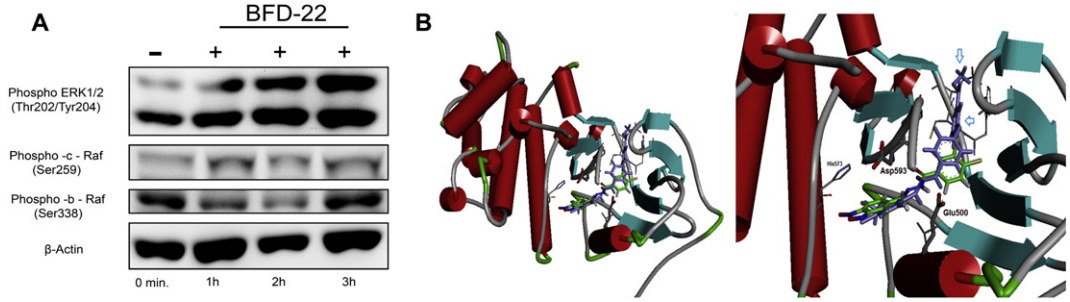

Fig. 4. (A) BFD-22 induces *in vitro* down-regulation of BRAF: B16F10 cells were treated with BDF-22 at the concentration of 8 μM for 1, 2 and 3 h and the phospho ERK 1/2 (Thr 202/Thr 204), C-RAF and BRAF levels were analyzed by Western blotting. β-Actin was used as loading control. (B) Schematic representation for the molecular docking of compound BDF-22 in the active site of BRAF (PDB ID 1UWH; Wan et al., 2004) using the Discovery Studio 4.0 Visualizer program (Accelrys Software Inc., 2005-13). The α-helices are presented as red cylinders and β-sheets are shown as cyan flat arrows. The BAY43-9006 co-crystallized inhibitor (sorafenib), which was used as the reference, is represented as stick model (all atoms in violet color). BFD-22 compound is also displayed as stick model, and the carbon atoms are in green, nitrogen in blue, oxygen in red, hydrogen atom in white, and chlorine in yellow. The amino acid residues in the active site are also shown as stick model. The inhibitors were similarly aligned in the interaction site of BRAF. The light blue arrows are indicating the region in the active site occupied by BAY43-9006 and not properly filled by BDF-22.

(sorafenib), co-crystallized with BRAF (PDB ID 1UWH; Wan et al., 2004). However, the *re*-docking energy values have shown that BFD-22 has less affinity for the BRAF active site than BAY43-9006, which presents lower energy score. In addition, BAY43-9006 is topologically larger than BFD-22, and because of that establishes more interactions with the amino acid residues in the active site (Fig. 4B). So, the optimization of BFD-22 should be considered in order to improve its binding into the BRAF protein.

3.6. BFD-22 inhibits lung metastasis in B16F10 melanoma model

In order to evaluate the *in vivo* antitumor efficacy of BFD-22, murine melanoma B16F10 cells were injected *via* the tail vein of C57BL6/J mice. A pilot study was performed in order to determine the time required for the development of the numbers of pulmonary non-lethal metastasis in living mice. Expansive nodules in the lungs were observed after 4 days of B16F10 cells injection. After that, B16F10 injected mice were randomized in four groups receiving the following treatments: intraperitoneal saline (control-vehicle), BFD-22 (40 mg/kg), sorafenib (10 mg/kg, positive control) and taxol (40 mg/kg, positive control). The treatment was started on day one after tumor cells inoculation. Animals were treated daily and, continuously, for 1 days in all treatment schedules. All treatments have inhibited lung metastasis in comparison to control mice. Anti-metastatic effects were strongest in animals that received BFD-22 treatment, ($^{**}p > 0.01$) when compared to those receiving sorafenib and taxol (Fig. 5).

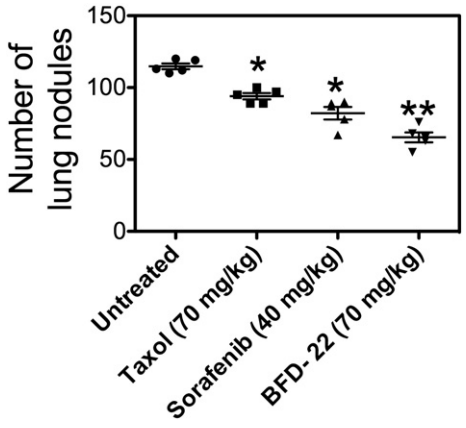

Fig. 5. Capacity of BFD-22 in inhibits lung metastasis on melanoma model. Lung colonization of B16F10 cells in a syngeneic system was used to evaluate the antitumor effects of BFD-22. The therapeutic activities of BFD-22 were evaluated by the daily injected intraperitoneally with dose of 70 mg/kg and were used taxol at the concentration of 70 mg/kg and sorafenib at the concentration of 40 mg/kg. Mice ($n = 5$/group) were challenged with 5×10^5 syngeneic B16F10 cells (0.1 ML/mouse). **, $p < 0.01$ by *t*-test.

3.7. BFD-22 simultaneously induces anti-tumor effects and presents immunomodulatory capacities

Ideally, new anticancer agents should provide direct anti-tumor effects, avoiding immunotoxicity while presenting immunomodulatory capacities (Menzies and Long, 2013). Therefore, it was investigated whether BFD-22 besides to have direct toxic effects on tumor cells could also have effect in some cells of the immune system. Firstly, the NO production by peritoneal macrophages was evaluated and was seen that BFD-22 enhanced NO production in a dose-dependent manner (Fig. 6A). Also, we have explored whether BDF-22 and sorafenib modulate bone marrow-derived dendritic cells (BMDC) activation, comparing treated cells to LPS-treated BMDCs, an agonist of Toll-like receptor 4 (TLR4). Of note, BMDC treated with BFD-22 (8 μM) have remained in cellular niches and maintained thin membrane projections, which are features of activated BMDCs (Fig. 6B). Furthermore, the exposure to BFD-22 or sorafenib did not have cytotoxic effects in macrophages, as evaluated by annexinV/PI double staining and live/dead staining (Fig. 6C and D). Additionally, even though immature BMDCs treated by BFD-22 did not show changes in the levels of I-A^b on their membrane (Henry et al., 2013), LPS-matured BMDCs, treated by BDF-22 up-regulated I-A^b on CD11c + cells (Neves et al., 2005; Park et al., 2014), suggesting that BFD-22 might stimulate DC maturation (Fig. 6E). Then, the question was if this feature would be reflected in the function of BMDCs to stimulate allogeneic T lymphocyte proliferation and it was found that BFD-22 treated BMDCs increased their potential to stimulate allogeneic T cell proliferation when compared to either untreated or sorafenib-treated cells. Also, immature BMDCs and LPS-matured BMDCs seems to stimulate higher frequencies of proliferating T lymphocytes (Fig. 6F). Together, these results suggest that BFD-22 might have immunomodulatory features without exerting toxic effects on immune system cells.

4. Discussion

In this study, we have provided the first evidence that benzofuroxan derivatives (BFDs) can be used as prototypes in cancer drug development. Our findings have shown that these compounds can cause cytotoxic effects against a variety of malignant tumor cells, and can be less cytotoxic on non-tumor cells (fibroblasts and melanocytes). It is noteworthy that among the tumor cell lines screened, the investigated compounds were more potent against melanoma cells, and compound **22**

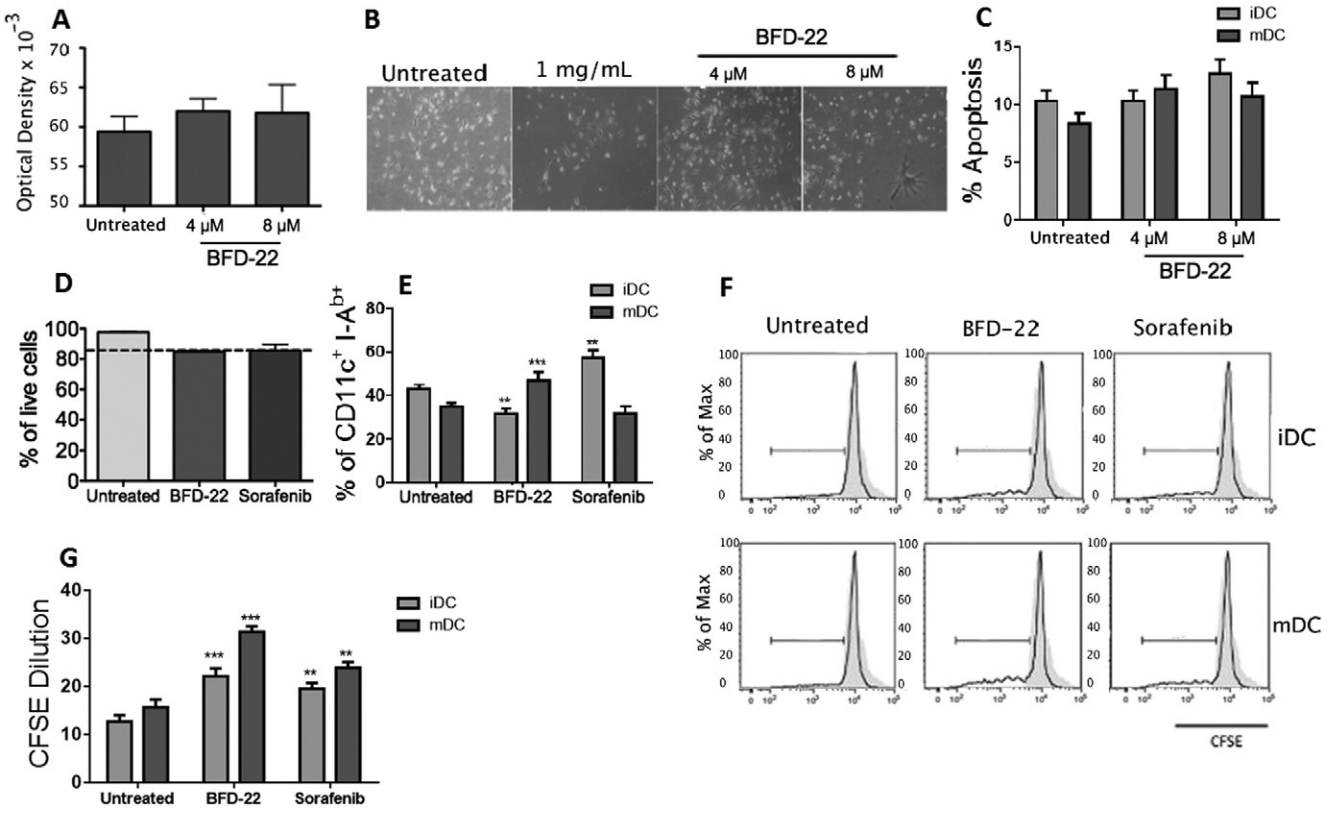

Fig. 6. BFD-22 induces anti-tumor effects and prevents immunotoxicity. (A) Peritoneal macrophage was treated with BFD-22 under different concentration. After 24 h, the supernatant was harvested and Nitric Oxide (NO) was measured by Griess reaction. (B) Representative picture of Bone Marrow dendritic cells (BMDC) without treatment or 24 h after treatment with BFD-22. (C) After 24 h treatment apoptosis was evaluated through AnexinV/PI staining measured by flow cytometry. (D) BMDCs were treated with the IC50 values of BFD-22 or sorafenib. After 24 h CD11c+ cells viability was evaluated by live-dead staining and measured by flow cytometry. (E) BMDCs treated with BFD-22 or sorafenib were challenged or not by LSP, wherein they were immature BMDC (iDC) or mature BMDC (mDC), respective. After 24 h, I-Ab was measured only in the living CD11c+ cells of both maturation states. (F) Representative picture of allogeneic T lymphocyte proliferation, wherein BMDCs were used to stimulated BALB/c lymphocytes. (G) BMDC iDC or mDC were harvested from culture and co-culture with allogeneic T lymphocytes, which were previously stained by CFSE since this dye dilution indicate cell proliferation, after 5 days culture, cells was harvested and CFSE dilution analyzed only in the CD3 population. Data are pooled from two independent experiments and values are mean ± SEM ($^{*}p < 0.01$, $^{**}p < 0.001$, $^{***}p < 0.0001$) was determined by ANOVA.

(BFD-22) has showed the highest activity against the B16F10 melanoma cells (Wild Type to BRAF) in comparison to the A2058 human melanoma (BRAF V600E mutant cell line). Then, BFD-22 can be, indeed, considered as a hit compound regarding this initial screening. The next step will be the optimization of the structural features through the rational design since the target is already known and the three-dimensional structure is available, in order to generate new chemical entities, which could effectively act on the wild and mutant BRAF protein. In this regard, the finding is quite important since the currently treatment options are limited for this highly aggressive and multi-chemoresistant tumor type (Gopal et al., 2014). BFD-22 has shown multiple effects against melanoma cells. The compound was able to induce cell cycle delay at the G1 phase and induce apoptosis. Indeed, migration and invasion were also observed. A highlight of this study is that BRAF protein might be a potential target for BDF-22. Most importantly, BFD-22 *in vivo* has inhibited melanoma growth and has presented immunomodulatory effect on BMDCs' ability to stimulate allogeneic T lymphocyte proliferation.

BFD-22 was cytotoxic to B16F10 melanoma cell lines, and the underlying mechanisms were investigated herein. Induction of apoptosis of cancer cells is the goal of many antitumor strategies in order to eliminate malignant cells. Our findings have revealed that the reduction of cell viability detected through MTT assay could be attributed to the induction of apoptosis in B16F10 cells by BFD-22. It is noteworthy that BFD-22 most likely activates the mitochondrial pathway during apoptosis because it seems to provoke a mitochondrial collapse known to trigger the intrinsic apoptotic pathway. Moreover, disruption of $\Delta\psi m$ has resulted in the activation of the executor caspase, caspase-3, which in turn can directly induce DNA fragmentation. The exact mechanism through which BFD-22 triggers apoptosis is still not fully understood. However, the increase in ROS production observed in BFD-22-treated melanoma cells probably would cause an oxidative stress, leading to dissipation of the proton gradient of the mitochondrial inner membrane, reducing $\Delta\psi m$, and ultimately leading to the induction of apoptosis in B16F10 cells. Notably, morphological changes typical of apoptosis, such as membrane blebbing, can be mediated by caspase-3 cleavage in B16F10 cells. Also, consistent with this mechanism, BFD-22 has decreased the cytoprotective effects of Hsp60 by inhibiting its ability to sequester the pro-apoptotic protein, Bax. In addition, BFD-22 has downregulated the expression of Bcl-2 in B16F10 cells, further indicating the priming of the mitochondrial apoptotic pathway (Ma et al., 2014). Then, taken the findings together, we propose that BFD-22 would act by activating the intrinsic apoptotic pathway by modulating the function of Bcl2-family members.

Furthermore, BFD-22 was able to inhibit cell migration and invasion *in vitro*, and metastatic spread of melanoma cells *in vivo*, which is an important goal in anti-melanoma treatment strategies. In addition, BFD-22 has decreased the expression of both syndecan and perlecan, which in turn prevents cell-matrix adhesion, indicating that BFD-22 would impair the ability of melanoma cells to adhere and anchor to the matrix. Moreover, BFD-22 has blocked B16F10 cell cycle progression.

Our data clearly have shown that the antiproliferative effects of BFD-22 can occur through the blockage of the cycle at the G0/G1 transition with a consequent reduction of proliferative G2/M phase. It is possible that BFD-22 could inhibit cell adhesion and invasion through the cell cycle arrest or, alternatively, by impairing matrix signaling. The

activation of the ERK1/2 pathway can attenuate DNA damage through the activation of the DNA repairing mechanism (Ellis et al., 2013). Surprisingly, BFD-22 has induced DNA fragmentation and up-regulation of pERK1/2 at the Thr202 and Tyr204 residues in B16F10 cells. Indeed, the ERK1/2 activation induced by BFD-22 could require p21/WAF1 leading to down-regulation of the CDK1 and cyclin B proteins, lacking cell cycle progression and inhibiting B16F10 cells proliferation. Besides that, BFD-22 has reduced the cyclin D1 and its catalytic partner CDK4, which in turn inhibits the formation of cyclin D1/CDK4. Thus, it can inhibit the progress of B16F10 cells through the cell cycle, preventing cell proliferation.

Pharmacological modulation of the mitogen-activated protein kinase (MAPK) pathway has been used to treat the metastatic stage IV of melanoma (Inamdar et al., 2010). Currently, the inhibition of BRAF is the established standard treatment for patients with melanoma. In this regard, vemurafenib has achieved favorable prognosis in mutant BRAF melanoma patients (Hu-Lieskovan et al., 2014). Herein, it was also investigated whether BRAF modulation could be involved in antitumor effects of BFD-22, and the first evidence was provided. BFD-22 can inhibit the BRAF/CRAF heterodimer formation, which could be associated with the interruption of RAF plasma membrane translocation, preventing ERK activation, and effectively inhibiting survival and proliferation of B16F10 cells. Furthermore, the BRAF downstream is related to until 2 h after BFD-22 treatment. However, it is reasonable to suggest that even BRAF having increased after 2 h, BFD-22 provoked a remarkable downstream in the MAPK/ERK kinase (MEK) signaling cascade. The major point regarding these results is that although BFD-22 has induced BRAF downstream for a shorter period, it was sufficient to down-regulate the RAF pathway and reduce melanoma cell proliferation. The therapeutic effects of BFD-22 were also investigated in a metastasis melanoma model in order to validate its anti-melanoma activity. Most importantly, BFD-22 has presented therapeutic effects as a single therapy. Indeed, BFD-22 is more effective for inhibiting lung tumor colonization than taxol and sorafenib. Furthermore, BFD-22 is more cytotoxic *in vitro* against B16F10 cells than taxol and sorafenib. In addition, the daily administration of BFD-22 for 15 days was well tolerated by mice. These *in vivo* remarkable effects of BFD-22 may not be only due to the down-regulation of BRAF, but also can indicate a target for BFD-22 in melanoma. In order to reinforce the experimental hypothesis, molecular docking studies were performed to investigate the binding mode of BFD-22 in the ATP catalytic site of BRAF kinase. Docking simulations have shown that BFD-22 fits well in the active site of BRAF, in an orientation similar to that observed for the co-crystalized inhibitor (BAY43-9006, sorafenib). The difference between the binding energy values of the two inhibitors was not significant (<5 kcal/mol). Furthermore, both molecules have established similar interactions with the amino acid residues Glu500 and Asp593 into the active site through two hydrogen bonding interactions: (i) *via* urea/hydrazide nitrogen atom to the carboxylate side chain of the catalytic Glu500 residue, and (ii) *via* carbonyl moiety to the main chain, on the nitrogen of Asp593, of the DFG (Asp593, Phe594, Gly595) motif. BFD-22, however, does not occupy the entire hydrophobic pocket of ATP adenine binding site as the inhibitor BAY43-9006 (the distal pyridyl ring). Then, molecular substitutions allowing the BFD-22 elongation in that portion of the molecule could increase its affinity for BRAF and improve its antitumor activity. Considering that, an assumption could be made: if BDF-22 is able to bind in the BRAF V600E active site there would be a down-regulation of RAS/BRAF/MEK/ERK pathway causing, then, the inhibition of cell proliferation and survival.

The immune system is responsible for tumor surveillance and long-term antitumor immunity. Potentially anticancer agents, ideally, should not damage the immunological components and instead, should cooperate with the system in order to join forces (Zitvogel et al., 2008; Barbuto, 2013). The effect of BFD-22 was evaluated over some cells of the immune system and we found that BMDCs treated with the compound were viable and morphologically preserved its main characteristic, the membrane projections. Of note, BFD-22 favored NO increase production by peritoneal macrophages and, used as stimuli for maturation along with LPS, BFD-22 was capable of improving BMDCs' capacity to stimulate allogeneic T lymphocytes proliferation. These findings suggest that BFD-22 might potentially modulate, thought its effect on professional antigen presenting cells, the antitumor immunity (Aranda et al., 2014; Pinho et al., 2014). However, more studies evaluating the effect of BFD-22 on the immune system are needed.

5. Conclusion

Summing up, data from this study have demonstrated that BFDs present cytotoxic to a variety of tumor cells. Among the investigated BFDs, we identified BFD-22 as an anti-melanoma hit. Also, BFD-22 has induced apoptosis of B16F10 cells by mitochondrial pathway. Indeed, cell cycle arrest is blocked due to inhibition of cyclin D1 and CDK4 activation. The data reported here provide the first evidence that BFD-22 can inhibit BRAF protein, and can provoke *in vitro* antiproliferative effects in B16F10 cells. Molecular docking studies have also supported the BRAF protein as a potential target for BDF-22. The BFD-22 binding mode is similar to sorafenib. The two inhibitors share the same orientation and type of interactions in the BRAF active site. Most important, our *in vivo* study has demonstrated that BFD-22 presents stronger antimetastatic effects, with superior therapeutic effects, when compared to sorafenib and taxol. Thus, the findings reported herein strongly support the pharmacological development of BFD-22 as a lead compound for the treatment of melanoma.

Competing interests.

All authors declare that they have no competing interests.

Acknowledgments

We acknowledge the grant support from Sao Paulo Research Foundation - (FAPESP), grant (2009/54599-5, 2013/07273-2, 2013/05396-0, 2014/07341-0 and 2014/14267-1) and Brazilian Governmental Agencies CNPq and CAPES.

References

Adams, C.P., Brantner, V.V., 2010. Spending on new drug development1. Health Econ. 19, 130–141.
Ahmed, A., Thliveris, J.A., Shaw, A., Sowa, M., Gilchrist, J., Scott, J.E., 2013. Caspase 3 activity in isolated fetal rat lung fibroblasts and rat periodontal ligament fibroblasts: cigarette smoke induced alterations. Tob. Induc. Dis. 11, 25.
Alexandre, G., Céline, V., Patrice, M., Carole, C.-M., Philippe, H., 2014. Effects of topical corticosteroids on cell proliferation, cell cycle progression and apoptosis: In vitro comparison on HaCaT. Int. J. Pharm.
Aranda, F., Bloy, N., Pesquet, J., Petit, B., Chaba, K., Sauvat, A., Kepp, O., Khadra, N., Enot, D., Pfirschke, C., 2014. Immune-dependent antineoplastic effects of cisplatin plus pyridoxine in non-small-cell lung cancer. Oncogene.
Barbuto, J.A.M., 2013. Are dysfunctional monocyte-derived dendritic cells in cancer an explanation for cancer vaccine failures? Immunotherapy 5, 105–107.
Berman, H.M., Westbrook, J., Feng, Z., Gilliland, G., Bhat, T., Weissig, H., Shindyalov, I.N., Bourne, P.E., 2000. The protein data bank. Nucleic Acids Res. 28, 235–242.
Boussabbeh, M., Salem, I.B., Prola, A., Guilbert, A., Bacha, H., Abid-Essefi, S., Lemaire, C., 2015. Patulin induces apoptosis through ROS-mediated endoplasmic reticulum stress pathway. Toxicol. Sci. kfu319.
Boussemart, L., Malka-Mahieu, H., Girault, I., Allard, D., Hemmingsson, O., Tomasic, G., Thomas, M., Basmadjian, C., Ribeiro, N., Thuaud, F., 2014. eIF4F is a nexus of resistance to anti-BRAF and anti-MEK cancer therapies. Nature 513, 105–109.
Brown, J.M., 1993. SR 4233 (tirapazamine): a new anticancer drug exploiting hypoxia in solid tumours. Br. J. Cancer 67, 1163.
Canon, J., Osgood, T., Olson, S.H., Saiki, A.Y., Robertson, R., Yu, D., Eksterowicz, J., Ye, Q., Jin, L., Chen, A., 2015. The MDM2 inhibitor AMG 232 demonstrates robust anti-tumor efficacy and potentiates the activity of p53-inducing cytotoxic agents. Mol. Cancer Ther. 0710 (2014).
Caputo, E., Miceli, R., Motti, M.L., Taté, R., Fratangelo, F., Botti, G., Mozzillo, N., Carriero, M.V., Cavalcanti, E., Palmieri, G., 2014. AurkA inhibitors enhance the effects of B-RAF and MEK inhibitors in melanoma treatment. J. Transl. Med. 12, 1–9.
Cerecetto, H., González, M., 2007. Benzofuroxan and furoxan. Chemistry and Biology, Bioactive Heterocycles IV. Springer, pp. 265–308.

Cerecetto, H., Porcal, W., 2005. Pharmacological properties of furoxans and benzofuroxans: recent developments. Mini Reviews in Medicinal Chemistry 5, 57–71.

Clavijo-Salomon, M.A., Ramos, R.N., Crippa, A., Pizzo, C.R., Bergami-Santos, P.C., Barbuto, J.A.M., 2014. Monocyte-derived dendritic cells reflect the immune functional status of a chromophobe renal cell carcinoma patient: could it be a general phenomenon? Cancer Immunology, Immunotherapy 1–11.

de Azevedo, R.A., Figueiredo, C.R., Ferreira, A.K., Matsuo, A.L., Massaoka, M.H., Girola, N., Auada, A.V., Farias, C.F., Pasqualoto, K.F., Rodrigues, C.P., 2014. Mastoparan induces apoptosis in B16F10-Nex2 melanoma cells *via* the intrinsic mitochondrial pathway and displays antitumor activity *in vivo*. Peptides.

Ellis, L., Ku, S., Ramakrishnan, S., Lasorsa, E., Azabdaftari, G., Godoy, A., Pili, R., 2013. Combinatorial antitumor effect of HDACs and the PI3K-Akt-mTOR pathway inhibition in a Pten deficient model of prostate cancer. Oncotarget 4, 2225.

Ferreira, A.K., Freitas, V.M., Levy, D., Ruiz, J.L.M., Bydlowski, S.P., Rici, R.E.G.R., Filho, O.M., Chierice, G.O., Maria, D.A., 2013. Anti-angiogenic and anti-metastatic activity of synthetic phosphoethanolamine. PLoS One 8, e57937.

Ferreira, A.K., de-Sá-Júnior, P.L., Pasqualoto, K.F.M., de Azevedo, R.A., Câmara, D.A.D., Costa, A.S., Figueiredo, C.R., Matsuo, A.L., Massaoka, M.H., Auada, A.V.V., 2014. Cytotoxic effects of dillapiole on MDA-MB-231 cells involve the induction of apoptosis through the mitochondrial pathway by inducing an oxidative stress while altering the cytoskeleton network. Biochimie 99, 195–207.

Freitas, V.M., do Amaral, J.B., Silva, T.A., Santos, E.S., Mangone, F.R., de Jesus Pinheiro, J., Jaeger, R.G., Nagai, M.A., Machado-Santelli, G.M., 2013. Decreased expression of ADAMTS-1 in human breast tumors stimulates migration and invasion. Mol. Cancer 12, 2.

Galluzzi, L., Bravo-San Pedro, J., Vitale, I., Aaronson, S., Abrams, J., Adam, D., Alnemri, E., Altucci, L., Andrews, D., Annicchiarico-Petruzzelli, M., 2015. Essential versus accessory aspects of cell death: recommendations of the NCCD 2015. Cell Death & Differentiation 22, 58–73.

Garg, M., 2015. Targeting microRNAs in epithelial-to-mesenchymal transition-induced cancer stem cells: therapeutic approaches in cancer. Expert Opinion on Therapeutic Targets 1–13.

Geeraerts, B., Vanhoecke, B., Berghe, W.V., Philippé, J., Offner, F., Deforce, D., 2007. Deguelin inhibits expression of IκBα protein and induces apoptosis of B-CLL cells in vitro. Leukemia 21, 1610–1618.

Ghosh, P., Whitehouse, M.W., 1968. Potential antileukemic and immunosuppressive drugs. Preparation and in vitro pharmacological activity of some 2, 1, 3-benzoxadiazoles (benzofurazans) and their N-oxides (benzofuroxans). J. Med. Chem. 11, 305–311.

Ghosh, J.C., Dohi, T., Kang, B.H., Altieri, D.C., 2008. Hsp60 regulation of tumor cell apoptosis. J. Biol. Chem. 283, 5188–5194.

Goetz, E.M., Ghandi, M., Treacy, D.J., Wagle, N., Garraway, L.A., 2014. ERK mutations confer resistance to mitogen-activated protein kinase pathway inhibitors. Cancer Res. 74, 7079–7089.

Gopal, Y.V., Rizos, H., Chen, G., Deng, W., Frederick, D.T., Cooper, Z.A., Scolyer, R.A., Pupo, G.M., Komurov, K., Sehgal, V., 2014. Inhibition of mTORC1/2 overcomes resistance to MAPK pathway inhibitors mediated by PGC1α and Oxidative Phosphorylation in melanoma. Cancer Research, Canres 1392.2014.

Henry, J.Y., Labarthe, M.C., Meyer, B., Dasgupta, P., Dalgleish, A.G., Galustian, C., 2013. Enhanced cross-priming of naive CD8+ T cells by dendritic cells treated by the IMiDs® immunomodulatory compounds lenalidomide and pomalidomide. Immunology 139, 377–385.

Hermann, F.J., Rodriguez Gomez, M., Doser, K., Edinger, M., Hoffmann, P., Schiechl, G., Talke, Y., Göbel, N., Schmidbauer, K., Brühl, H., 2014. Basophils inhibit proliferation of CD4+ T cells in autologous and allogeneic mixed lymphocyte reactions and limit disease activity in a murine model of graft versus host disease. Immunology.

Hjerpe, E., Egyhazi, S., Carlson, J., Stolt, M.F., Schedvins, K., Johansson, H., Shoshan, M., Åvall-Lundqvist, E., 2013. HSP60 predicts survival in advanced serous ovarian cancer. Int. J. Gynecol. Cancer 23, 448–455.

Hu-Lieskovan, S., Robert, L., Moreno, B.H., Ribas, A., 2014. Combining targeted therapy with immunotherapy in BRAF-mutant melanoma: promise and challenges. J. Clin. Oncol. 32, 2248–2254.

Inamdar, G.S., Madhunapantula, S.V., Robertson, G.P., 2010. Targeting the MAPK pathway in melanoma: why some approaches succeed and other fail. Biochem. Pharmacol. 80, 624–637.

Jandova, J., Mason, C., Pawar, S., Watts, G., 2014. Fn14 receptor promotes invasive potential and metastatic capacity of non-small lung adenocarcinoma cells through the up-regulation of integrin α6. Neoplasma 62, 41–52.

Johnson, D.B., Flaherty, K.T., Weber, J.S., Infante, J.R., Kim, K.B., Kefford, R.F., Hamid, O., Schuchter, L., Cebon, J., Sharfman, W.H., 2014. Combined BRAF (Dabrafenib) and MEK inhibition (Trametinib) in patients With BRAFV600-mutant melanoma experiencing progression with single-agent BRAF inhibitor. Journal of Clinical Oncology, JCO 2014.2057. 3535.

Jorge, S.D., Masunari, A., Rangel-Yagui, C.O., Pasqualoto, K.F.M., Tavares, L.C., 2009. Design, synthesis, antimicrobial activity and molecular modeling studies of novel benzofuroxan derivatives against *Staphylococcus aureus*. Bioorg. Med. Chem. 17, 3028–3036.

Jorge, S.D., Palace-Berl, F., Masunari, A., Cechinel, C.A., Ishii, M., Pasqualoto, K.F.M., Tavares, L.C., 2011. Novel benzofuroxan derivatives against multidrug-resistant *Staphylococcus aureus* strains: design using Topliss' decision tree, synthesis and biological assay. Bioorganic & medicinal chemistry 19, 5031–5038.

Jorge, S.D., Ishii, M., Palace-Berl, F., Ferreira, A.K., de Sa Junior, P.L., de Oliveira, A.A., Sonehara, I.Y., Pasqualoto, K.F.M., Tavares, L.C., 2012. Preliminary in vitro evaluation of N′-(benzofuroxan-5-yl) methylene benzohydrazide derivatives as potential anti-Trypanosoma cruzi agents. Med. Chem. Comm. 3, 824–828.

Jorge, S.D., Palace-Berl, F., Mesquita Pasqualoto, K.F., Ishii, M., Ferreira, A.K., Berra, C.M., Bosch, R.V., Maria, D.A., Tavares, L.C., 2013. Ligand-based design, synthesis, and experimental evaluation of novel benzofuroxan derivatives as anti-*Trypanosoma cruzi* agents. Eur. J. Med. Chem. 64, 200–214.

Joseph, J., Conroy, S., Tomar, T., Eggens-Meijer, E., Bhat, K., Copray, S., Walenkamp, A., Boddeke, E., Balasubramanyian, V., Wagemakers, M., 2014. TGF-β is an inducer of ZEB1-dependent mesenchymal transdifferentiation in glioblastoma that is associated with tumor invasion. Cell Death Dis. 5, e1443.

Jovene, C., Chugunova, E.A., Goumont, R., 2013. The properties and the use of substituted benzofuroxans in pharmaceutical and medicinal chemistry: a comprehensive review. Mini Rev. Med. Chem. 13, 1089–1136.

Lam, T.S., de Meent, M., Falkenburg, J., Jedema, I., 2014. Monocyte-derived dendritic cells can induce autoreactive CD4+ T cells showing myeloid lineage-directed reactivity in healthy individuals. Eur. J. Immunol.

Lens, M., Dawes, M., 2004. Global perspectives of contemporary epidemiological trends of cutaneous malignant melanoma. Br. J. Dermatol. 150, 179–185.

Li, L., Zhang, Q., Ding, Y., Jiang, H., Thiers, B.H., Wang, J.Z., 2014. Automatic diagnosis of melanoma using machine learning methods on a spectroscopic system. BMC Med. Imaging 14, 36.

Long, G.V., Stroyakovskiy, D., Gogas, H., Levchenko, E., de Braud, F., Larkin, J., Garbe, C., Jouary, T., Hauschild, A., Grob, J.J., 2014. Combined BRAF and MEK inhibition versus BRAF inhibition alone in melanoma. N. Engl. J. Med. 371, 1877–1888.

Lu, T.-H., Tseng, T.-J., Su, C.-C., Tang, F.-C., Yen, C.-C., Liu, Y.-Y., Yang, C.-Y., Wu, C.-C., Chen, K.-L., Hung, D.-Z., 2014. Arsenic induces reactive oxygen species-caused neuronal cell apoptosis through JNK/ERK-mediated mitochondria-dependent and GRP 78/CHOP-regulated pathways. Toxicol. Lett. 224, 130–140.

Ma, S., Nguyen, T., Tan, I., Ninnis, R., Iyer, S., Stroud, D., Menard, M., Kluck, R., Ryan, M., Dewson, G., 2014. Bax targets mitochondria by distinct mechanisms before or during apoptotic cell death: a requirement for VDAC2 or Bak for efficient Bax apoptotic function. Cell Death Differ.

Mader, M., 2005. Novel antiproliferative antitumor agents. Curr. Opin. Drug Discov. Devel. 8, 613–618.

Martin, S.K., Kamelgarn, M., Kyprianou, N., 2014. Featured review article cytoskeleton targeting value in prostate cancer treatment. Am. J. Clin. Exp. Urol. 2, 15–26.

Menzies, A.M., Long, G.V., 2013. Recent advances in melanoma systemic therapy. BRAF inhibitors, CTLA4 antibodies and beyond. Eur. J. Cancer 49, 3229–3241.

Monge-Fuentes, V., Muehlmann, L.A., de Azevedo, R.B., 2014. Perspectives on the application of nanotechnology in photodynamic therapy for the treatment of melanoma. Nano Rev. 5.

Morris, G.M., Goodsell, D.S., Halliday, R.S., Huey, R., Hart, W.E., Belew, R.K., Olson, A.J., 1998. Automated docking using a Lamarckian genetic algorithm and an empirical binding free energy function. J. Comput. Chem. 19, 1639–1662.

Morris, G.M., Huey, R., Lindstrom, W., Sanner, M.F., Belew, R.K., Goodsell, D.S., Olson, A.J., 2009. AutoDock4 and AutoDockTools4: automated docking with selective receptor flexibility. J. Comput. Chem. 30, 2785–2791.

Naselli, F., Tesoriere, L., Caradonna, F., Bellavia, D., Attanzio, A., Gentile, C., Livrea, M.A., 2014. Anti-proliferative and pro-apoptotic activity of whole extract and isolated indicaxanthin from *Opuntia ficus-indica* associated with re-activation of the onco-suppressor p16 ^{INK4a} gene in human colorectal carcinoma (Caco-2) cells. Biochem. Biophys. Res. Commun. 450, 652–658.

Neves, A.R., Ensina, L.F.C., Anselmo, L.B., Leite, K.R., Buzaid, A.C., Câmara-Lopes, L.H., Barbuto, J.A.M., 2005. Dendritic cells derived from metastatic cancer patients vaccinated with allogeneic dendritic cell–autologous tumor cell hybrids express more CD86 and induce higher levels of interferon-gamma in mixed lymphocyte reactions. Cancer Immunol. Immunother. 54, 61–66.

Park, H., Huang, X., Lu, C., Cairo, M.S., Zhou, X., 2014. miR-146a and miR-146b Regulate Human Dendritic Cell Apoptosis and Cytokine Production by Targeting of TRAF6 and IRAK1. J. Biol. Chem. M114. 591420.

Pinho, M.P., Migliori, I.K., Flatow, E.A., Barbuto, J.A.M., 2014. Dendritic cell membrane CD83 enhances immune responses by boosting intracellular calcium release in T lymphocytes. J. Leukoc. Biol. 95, 755–762.

Qi, H.-w., Xin, L.-y., Xu, X., Ji, X.-x., Fan, L.-h., 2014. Epithelial-to-mesenchymal transition markers to predict response of Berberine in suppressing lung cancer invasion and metastasis. J. Transl. Med. 12, 22.

Richardson, M., Ayliffe, M., Helbert, M., Davies, E., 1998. A simple flow cytometry assay using dihydrorhodamine for the measurement of the neutrophil respiratory burst in whole blood: comparison with the quantitative nitrobluetetrazolium test. J. Immunol. Methods 219, 187–193.

Sarangi, U., Singh, M.K., Abhijnya, K.V.V., Reddy, L.P.A., Prasad, B.S., Pitke, V.V., Paithankar, K., Sreedhar, A.S., 2013. Hsp60 chaperonin acts as barrier to pharmacologically induced oxidative stress mediated apoptosis in tumor cells with differential stress response. Drug Target Insights 7, 35.

Šarlauskas, J., Miliukienė, V., Anusevičius, Ž., Misevičienė, L., Krikštopaitis, K., Nemeikaitė-Čėnienė, A., Vitėnienė, I., Čėnas, N., 2009. Redox properties and prooxidant cytotoxicity of benzofuroxans: a comparison with nitrobenzenes. Chemija 20, 109–115.

Shen, H., Zeng, G., Tang, G., Cai, X., Bi, L., Huang, C., Yang, Y., 2014. Antimetastatic effects of licochalcone A on oral cancer via regulating metastasis-associated proteases. Tumor Biology 1–8.

Smith, M.P., Sanchez-Laorden, B., O'Brien, K., Brunton, H., Ferguson, J., Young, H., Dhomen, N., Flaherty, K.T., Frederick, D.T., Cooper, Z.A., 2014. The immune microenvironment confers resistance to MAPK pathway inhibitors through macrophage-derived TNFα. Cancer Discovery 4, 1214–1229.

Teixeira, S.F., de Azevedo, R.A., Salomon, M.A.C., Jorge, S.D., Levy, D., Bydlowski, S.P., Rodrigues, C.P., Pizzo, C.R., Barbuto, J.A.M., Ferreira, A.K., 2014. Synergistic antitumor effects of the combination of a benzofuroxan derivate and sorafenib on NCI-H460 human large cell lung carcinoma cells. Biomed. Pharmacother.

Thyrell, L., Erickson, S., Zhivotovsky, B., Pokrovskaja, K., Sangfelt, O., Castro, J., Einhorn, S., Grander, D., 2002. Mechanisms of Interferon-alpha induced apoptosis in malignant cells. Oncogene 21, 1251–1262.

Tomei, S., Bedognetti, D., De Giorgi, V., Sommariva, M., Civini, S., Reinboth, J., Al Hashmi, M., Ascierto, M.L., Liu, Q., Ayotte, B.D., 2014. The immune-related role of BRAF in melanoma. Mol. Oncol.

van Dijk, M., Göransson, S.A., Strömblad, S., 2013. Cell to extracellular matrix interactions and their reciprocal nature in cancer. Exp. Cell Res. 319, 1663–1670.

Wada, M., Horinaka, M., Yamazaki, T., Katoh, N., Sakai, T., 2014. The dual RAF/MEK inhibitor CH5126766/RO5126766 may be a potential therapy for RAS-Mutated tumor cells. PLoS One 9, e113217.

Wan, P.T., Garnett, M.J., Roe, S.M., Lee, S., Niculescu-Duvaz, D., Good, V.M., Project, C.G., Jones, C.M., Marshall, C.J., Springer, C.J., 2004. Mechanism of activation of the RAF-ERK signaling pathway by oncogenic mutations of B-RAF. Cell 116, 855–867.

Weise, A.M., Flaherty, L.E., 2014. New options for the adjuvant treatment of cutaneous melanoma? Curr. Oncol. Rep. 16, 1–6.

Wevers, K., Hoekstra, H., 2013. Stage IV melanoma: completely resectable patients are scarce. Ann. Surg. Oncol. 20, 2352–2356.

Xie, Q., Tang, N., Lin, Y., Wang, X., Lin, X., Lin, J., 2013. Recombinant adenovirus snake venom cystatin inhibits the growth, invasion, and metastasis of B16F10 cells in vitro and in vivo. Melanoma Res. 23, 444–451.

Xu, W., Cheng, M., Lao, Y., Wang, X., Wu, J., Zhou, L., Zhang, Y., Xu, H., Xu, N., 2015. DNA damage and ER stress contribute to oblongifolin C-induced cell killing in Bax/Bak-deficient cells. Biochemical and Biophysical Research Communications.

Ye, L., Yuan, G., Xu, F., Sun, Y., Chen, Z., Chen, M., Li, T., Sun, P., Li, S., Sun, J., 2014. The small-molecule compound BM-1197 inhibits the antiapoptotic regulators Bcl-2/Bcl-xL and triggers apoptotic cell death in human colorectal cancer cells. Tumor Biol. 1-9.

Zhou, Y., Shu, F., Liang, X., Chang, H., Shi, L., Peng, X., Zhu, J., Mi, M., 2014. Ampelopsin induces cell growth inhibition and apoptosis in breast cancer cells through ROS Generation and endoplasmic reticulum stress pathway. PLoS One 9, e89021.

Zitvogel, L., Apetoh, L., Ghiringhelli, F., André, F., Tesniere, A., Kroemer, G., 2008. The anticancer immune response: indispensable for therapeutic success? J. Clin. Invest. 118, 1991–2001.